AIAA JOURNAL
Vol. 42, No. 6, June 2004

Effect of Delamination on Active Constrained Layer Damping of Smart Composite Beams

M. C. Ray* and J. N. Reddy†
Texas A&M University, College Station, Texas 77843-3123

A novel work demonstrates the effect of delamination in smart laminated composite beams on the performance of active constrained layer damping (ACLD) treatment. A finite element model has been derived to formulate the dynamics of the composite beams integrated with a patch of ACLD treatment and a patch of piezoelectric film acting as a distributed sensor with and without the presence of delamination at different locations. Frequency response functions of the beams have been examined to observe the effect of delamination on the performance of ACLD treatment. It has been observed that the ACLD treatment improves the active damping characteristics of the beams, even in the presence of delamination, and that the responses of the beams are sensitive to the variation of the location of delamination. The responses due to active constrained layer damping presented may provide a useful guide to detect the presence of delamination in smart composite beams by the use of the existing numerical techniques.

Nomenclature

a	=	length of composite beams
a_e	=	length of an element
$[B_b]$, $[B_s]$	=	nodal strain–displacement matrices
b	=	width of composite beams
$[C_d]$	=	active damping matrix
$[C^L]$	=	elastic coefficient matrix for Lth layer
$\{D_{ap}\}$	=	electroelastic rigidity matrix
$[D_b]$, $[D_s]$	=	rigidity matrices
D_z	=	electric displacement in z direction
$\{d\}$, $\{d^e\}$	=	generalized and nodal generalized displacement vectors
E	=	Young's modulus of viscoelastic material
E_z	=	electric field in z direction
E_1, E_3	=	orthotropic elastic moduli of composite materials
e_{31}	=	piezoelectric stress coefficient
$\{F^e\}$, $\{F\}$	=	elemental and global nodal force vectors
$\{F_a^e\}$, $\{F_a\}$	=	elemental and global electroelastic coupling matrices
G	=	complex shear modulus of the viscoelastic material
G_{13}	=	orthotropic shear modulus of the composite materials
h, h_p, h_c	=	thicknesses of composite beams, piezoelectric layer, and viscoelastic layer
i	=	index for node number of an element
K_d	=	control gain
$[K^e]$, $[K]$	=	elemental and global stiffness matrices
$[K^e_{\text{sen}}]$	=	elemental electroelastic coupling matrix for sensor
L	=	index for layer number
$[M^e]$, $[M]$	=	elemental and global mass matrices
$\bar{m}$	=	mass parameter
N	=	number of layers in the composite beams
$[N]$	=	shape function matrix
n_i	=	shape function for ith node of an element
p	=	time harmonic external excitation
q, q^e	=	total, elemental induced charge per unit width of the sensor layer
$[r]$	=	position vector
T_k, T_k^e	=	total, elemental kinetic energies
T_p, T_p^e	=	total, elemental potential energies
u	=	axial displacement in x direction
u_0	=	generalized translational displacement in x direction
V	=	control voltage
w	=	transverse displacement
(x, y, z)	=	Cartesian coordinates
x_1, x_2	=	x coordinates of start and end of delamination
z_c	=	z coordinate of the middle layer of sublaminates
Δ	=	displacement vector
ε_x, ε_{xz}	=	normal, transverse shear strains
η	=	loss factor of the viscoelastic material
θ_x	=	generalized rotation
σ_x, σ_{xz}	=	normal, transverse shear stresses
ρ^L	=	mass density of Lth layer

I. Introduction

USE of piezoelectric materials for distributed actuators and sensors has attained a great deal of importance toward the development of high-performing lightweight smart structures.[1–20] With proper control voltage, the distributed piezoelectric actuators artificially incorporate damping into the structures in response to the external stimuli resulting in active control of the structure. The measure of the active damping characteristics depends on the magnitude of the piezoelectric stress/strain constants. However, the magnitudes of the piezoelectric constants of the currently available piezoelectric materials are very low. Hence, large control voltage is necessary for achieving a significant amount of damping, which may be the limiting factor for commercially viable designs, as well as for the existing piezoelectric materials. Further research on the improvement of the active damping characteristics of the lightweight structures using piezoelectric materials led to the development of active constrained layer damping (ACLD) treatment.[21] The ACLD treatment consists of a piezoelectric constraining layer and a constrained viscoelastic layer. By properly activation of the piezoelectric constraining layer of the ACLD treatment, the transverse shear deformations of the viscoelastic layer can be increased over its passive counterpart, resulting in improved damping characteristics of the flexible structures. Because the passive damping mechanism is integral to the ACLD treatment, active constrained layer damping provides the attributes of both passive and active damping. Because the control effort necessary to increase the shear deformation of the viscoelastic layer is compatible with the low control authority of the currently available piezoelectric materials, the ACLD treatment may be a practical

Received 13 August 2002; revision received 24 January 2003; accepted for publication 13 January 2004.

*Visiting Associate Professor, Mechanical Engineering Department.
†Distinguished Professor, Mechanical Engineering Department.

means for active control of light weight smart structures without the need for high control voltage. As a result, since its inception, extensive research has been carried out to investigate the effectiveness of ACLD treatment in achieving the improved damping characteristics of beams, plates, and shells made of isotropic materials.[21–30]

Recently, laminated structures of composite materials have been considered for the load bearing part of the smart structures.[7,15,19] Although the laminated structures of composite materials provide high stiffness to weight ratio, these structures develop imperfections while under operation due to several causes not mentioned here. One of the serious imperfections is the formation of delaminations in the laminated structures. The effect of delamination on the performance of smart laminated composite structures would be an important issue, such that the delamination can be detected at its early stage. Extensive efforts are being exerted toward the development of a nondestructive health-monitoring technique to detect delaminations in the composite structures.[31–36] It has been reported that the structural damage detection can best be performed by the use of frequency response function (FRF) data.[35] Hence, the affected FRF data due to the onslaught of delaminations are a prerequisite for the detection of delamination in the laminated smart composite structures. Thus far, only one paper[37] on the analysis of delaminated smart composite beams is currently available. However, this paper is not concerned with the frequency domain analysis, and, moreover, the paper does not reveal any significantly affected time response due to the presence of delamination. This may be because low control authority piezoelectric patches have been used alone as the actuator, resulting in low active damping characteristics.

In this paper, an endeavor has been made to investigate the effect of delamination in smart laminated composite beams on the performance of ACLD treatment. The beams considered here are integrated with a patch of ACLD treatment and a piezoelectric layer acting as a patch-type sensor. A simple finite element model has been derived to study the dynamic behavior of the beams in the frequency domain with or without delamination. Emphasis is placed on examination of the active frequency responses of the beams in the presence of delamination at different locations. The response may be useful for the purpose of detection and location of the delaminations in smart composite beams using the already existing technique.[35]

II. Theoretical Formulation

In this section, the equations of motion governing the open-loop behavior of laminated composite beams, with or without delaminations, and integrated with a patch of ACLD treatment, are derived. Figure 1 is a schematic diagram of such a cantilever beam coupled with a patch of ACLD treatment on its top surface. A patch of piezoelectric layer is also attached at the bottom surface of the beam that acts as a sensor layer. The beam is made of N number of orthotropic layers. The length, width, and the thickness of the beam are represented by a, b, and h, respectively. The thickness of the piezoelectric layers and that of the viscoelastic layer are denoted by h_p and h_c, respectively. The z coordinates of the middle surfaces of the sublaminates above and below the delamination are designated by z_1 and z_2, respectively. The middle surfaces of the undelaminated portions of the beam coincide with the reference plane ($z = 0$). The strain energy and mass of the thin piezoelectric sensor layer may be assumed to be negligibly small and will not be considered in the estimation of the potential and kinetic energies of the overall system. Hence, the layer numbering has been considered to start from the bottom-most layer of the composite base beam.

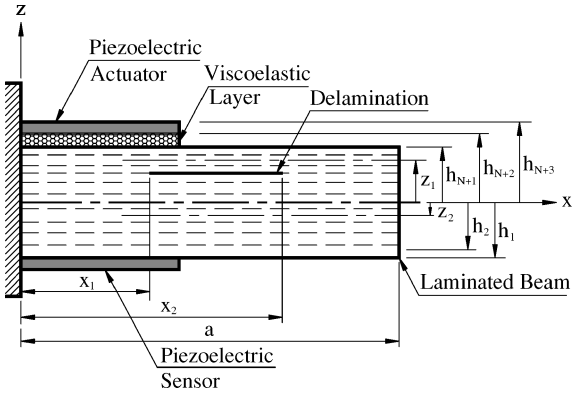

Fig. 1 Schematic diagram of a laminated composite beam integrated with a patch of ACLD treatment and a sensor layer.

A. Displacement Field

The laminated composite beams considered in this study for the base structure of the smart beams are highly thin. Hence, first-order shear deformation theory has been considered to model the kinematics of deformation. Accordingly, the longitudinal displacement u of any point belonging to a sublaminate located either in the delaminated zone ($x_1 \le x \le x_2$), or in the undelaminated zone ($0 \le x \le x_1$ or $x_2 \le x \le a$) of the beam, integrated with the patch of ACLD treatment, can be written as

$$u(x, z, t) = u_0(x, t) + (z - z_c)\theta_x(x, t) \tag{1}$$

In Eq. (1), u_0 is the generalized translational displacement at any point on the middle surface of the sublaminate in concern, θ_x is the rotation of the normal to this middle plane in x–z plane, and z_c represents the z coordinate of the middle surface of the zone. Because the transverse normal strain is usually considered as negligible for thin structures, the transverse displacement w is assumed to be constant through the thickness of the beam, viscoelastic layer, and the piezoelectric layers.

B. Strain–Displacement Relations

It is assumed that the delamination does not open during the vibratory motion of the beam. Thus, by the use of linear strain–displacement relations and Eq. (1), the normal strain ε_x and the transverse shear strain ε_{xz} at any point in the overall beam continuum can be written as

$$\varepsilon_x = \frac{\partial u_0}{\partial x} + (z - z_c)\frac{\partial \theta_x}{\partial x}, \qquad \varepsilon_{xz} = \frac{\partial w}{\partial x} + \theta_x \tag{2}$$

C. Constitutive Relations

The constitutive equations for the materials of orthotropic layers of the laminated beams are

$$\{\sigma^L\} = [C^L]\{\varepsilon^L\}, \qquad L = 1, 2, 3, \ldots, N \tag{3}$$

in which $[C^L]$ is the elastic constants matrix of the Lth layer, and the vectors $\{\sigma\}$ and $\{\varepsilon\}$, defining, respectively, the state of stress and strain at a point, are given by

$$\{\sigma\} = [\sigma_x \quad \sigma_{xz}]^T, \qquad \{\varepsilon\} = [\varepsilon_x \quad \varepsilon_{xz}]^T \tag{4}$$

where σ_x is the normal stress in the x direction and σ_{xz} is the transverse shear stress. The stress–strain relations for the material of the piezoelectric layer are

$$\{\sigma^L\} = [C^L]\{\varepsilon^L\} - [e]^T E_z, \qquad L = N + 2 \tag{5}$$

in which E_z is the applied electric field in the z direction, and, for the piezoelectric material considered here, the vector of piezoelectric stress constants $[e]$ is given by

$$[e] = [e_{31} \quad 0] \tag{6}$$

wherein e_{31} is the piezoelectric stress constant quantifying the induced stress in the x direction due to unit electric field in the z direction.

The material of the viscoelastic layer is assumed to be linearly viscoelastic and isotropic. Because the present study is concerned with the frequency response analysis, the viscoelastic material can be modeled by the use of the commonly used complex modulus approach, which is a frequency-domain-based model. In the complex

modulus approach, the shear modulus $\boldsymbol{G}$ and Young's modulus $\boldsymbol{E}$ of the viscoelastic material are described by[26,28]

$$\boldsymbol{G} = \boldsymbol{G}'(1 + j\eta), \qquad \boldsymbol{E} = 2\boldsymbol{G}(1 + \upsilon) \tag{7}$$

in which $\boldsymbol{G}'$ is the storage modulus, υ is the Poisson's ratio, η is the loss factor at a particular operating temperature and frequency, and $j = \sqrt{-1}$. Accordingly, the elastic constant matrix $[\boldsymbol{C}]$ of the viscoelasctic material becomes complex, and, for $\boldsymbol{L} = \boldsymbol{N} + 1$, Eq. (3) also represents the constitutive equations for the viscoelastic material.[26,28,38]

D. Continuity Conditions

The axial displacements are continuous at the interface between the sublaminate in the delaminated zone and the sublaminate in the healthy zone. Hence, the present model must satisfy the following interface continuity conditions:

$$\begin{aligned} \boldsymbol{u}(\boldsymbol{x}_1, z, t)|_{\text{undelaminated}} &= \boldsymbol{u}(\boldsymbol{x}_1, z, t)|_{\text{delaminated}} \\ \boldsymbol{u}(\boldsymbol{x}_2, z, t)|_{\text{undelaminated}} &= \boldsymbol{u}(\boldsymbol{x}_2, z, t)|_{\text{delaminated}} \end{aligned} \tag{8}$$

E. Finite Element Model

The total potential energy $\boldsymbol{T}_p$ and the kinetic energy $\boldsymbol{T}_k$ of the overall system are given by

$$\boldsymbol{T}_p = \frac{1}{2}\boldsymbol{b}\sum_{L=1}^{N+2}\int_{h_L}^{h_{L+1}}\int_0^a \left(\sigma_x^L \varepsilon_x^L + \sigma_{xz}^L \varepsilon_{xz}^L\right) \mathrm{d}\boldsymbol{x}\,\mathrm{d}z - \boldsymbol{b}\int_0^a \boldsymbol{p}(\boldsymbol{x}, t)\boldsymbol{w}\,\mathrm{d}\boldsymbol{x} \tag{9}$$

$$\boldsymbol{T}_k = \frac{1}{2}\boldsymbol{b}\sum_{L=1}^{N+2}\int_{h_L}^{h_{L+1}}\int_0^a \rho^L \{\dot{\boldsymbol{\Delta}}^L\}^T\{\dot{\boldsymbol{\Delta}}^L\}\,\mathrm{d}\boldsymbol{x}\,\mathrm{d}z \tag{10}$$

in which $\boldsymbol{p}(\boldsymbol{x}, t)$ is the externally applied distributed load in the z direction, ρ^L is the density of the $\boldsymbol{L}$th layer, and $\{\boldsymbol{\Delta}\}$ is the vector of displacements $(\boldsymbol{u}, \boldsymbol{w})$ at any point in the layer. The dot over a quantity indicates the derivative of the quantity with respect to time. The whole continuum is discretized by a three-noded one-dimensional isoparametric element. By definition of the generalized displacement vector $\{\boldsymbol{d}\}$ at any point as

$$\{\boldsymbol{d}\} = [\boldsymbol{u}_0 \quad \boldsymbol{w} \quad \boldsymbol{\theta}_x]^T \tag{11}$$

the generalized displacement vector at any point within the element can be expressed as

$$\{\boldsymbol{d}\} = [\boldsymbol{N}]\{\boldsymbol{d}^e\} \tag{12}$$

In Eq. (12), the nodal generalized degrees of freedom $\{\boldsymbol{d}^e\}$ and the shape function matrix $[\boldsymbol{N}]$ of the element are given by

$$\{\boldsymbol{d}^e\} = \left[\{\boldsymbol{d}_1\}^T \quad \{\boldsymbol{d}_2\}^T \quad \{\boldsymbol{d}_3\}^T\right]^T$$

$$\{\boldsymbol{d}_i\} = [\boldsymbol{u}_{0i} \quad \boldsymbol{w}_i \quad \boldsymbol{\theta}_{xi}]^T, \qquad \boldsymbol{i} = 1, 2, 3$$

$$[\boldsymbol{N}] = \begin{bmatrix} \boldsymbol{n}_1 & 0 & 0 & \boldsymbol{n}_2 & 0 & 0 & \boldsymbol{n}_3 & 0 & 0 \\ 0 & \boldsymbol{n}_1 & 0 & 0 & \boldsymbol{n}_2 & 0 & 0 & \boldsymbol{n}_3 & 0 \\ 0 & 0 & \boldsymbol{n}_1 & 0 & 0 & \boldsymbol{n}_2 & 0 & 0 & \boldsymbol{n}_3 \end{bmatrix}$$

where $\boldsymbol{n}_i$, $\boldsymbol{i} = 1, 2, 3$, is the shape function associated with the node $\boldsymbol{i}$ of the element. By the use of Eq. (12) in relations (2) and (3), the normal and transverse shear strains at any point within the element can be expressed as

$$\varepsilon_x = [\boldsymbol{Z}][\boldsymbol{B}_b]\{\boldsymbol{d}^e\}, \qquad \varepsilon_{xz} = [\boldsymbol{B}_s]\{\boldsymbol{d}^e\} \tag{13}$$

where

$$[\boldsymbol{Z}] = [1 \quad (z - z_c)], \qquad [\boldsymbol{B}_b] = [\boldsymbol{B}_{b1} \quad \boldsymbol{B}_{b2} \quad \boldsymbol{B}_{b3}]$$

$$[\boldsymbol{B}_s] = [\boldsymbol{B}_{s1} \quad \boldsymbol{B}_{s2} \quad \boldsymbol{B}_{s3}]$$

The various submatrices in $[\boldsymbol{B}_b]$ and $[\boldsymbol{B}_s]$ are obtained as

$$[\boldsymbol{B}_{bi}] = \begin{bmatrix} \boldsymbol{n}_{i,x} & 0 & 0 \\ 0 & 0 & \boldsymbol{n}_{i,x} \end{bmatrix}, \qquad [B_{si}] = [\,0 \quad \boldsymbol{n}_{i,x} \quad \boldsymbol{n}_i\,]$$

$$\boldsymbol{n}_{i,x} = \frac{\partial \boldsymbol{n}_i}{\partial \boldsymbol{x}}, \qquad \boldsymbol{i} = 1, 2, 3$$

When Eqs. (3–6) and (13) are substituted into Eqs. (9) and (10), the potential energy $\boldsymbol{T}_p^e$ of the $\boldsymbol{e}$th typical beam element augmented with the ACLD treatment can be expressed as

$$\begin{aligned} \boldsymbol{T}_p^e = \frac{1}{2}\boldsymbol{b}\int_0^{a_e} \Big[&\{\boldsymbol{d}^e\}^T([\boldsymbol{B}_b]^T[\boldsymbol{D}_b][\boldsymbol{B}_b] + [\boldsymbol{B}_s]^T[\boldsymbol{D}_s][\boldsymbol{B}_s])\{\boldsymbol{d}^e\} \\ &- \{\boldsymbol{d}^e\}^{\boldsymbol{T}}[\boldsymbol{B}_b]^T\{\boldsymbol{D}_{ap}\}\boldsymbol{V} - 2\{\boldsymbol{d}^e\}^T[\boldsymbol{N}]^T\{\boldsymbol{f}^s\}\Big]\,\mathrm{d}\boldsymbol{x} \end{aligned} \tag{14}$$

and the kinetic energy $\boldsymbol{T}_k^e$ of the element can be written as

$$\boldsymbol{T}_k^e = \frac{1}{2}\boldsymbol{b}\int_0^{a_e} \{\dot{\boldsymbol{d}}^e\}^T[\boldsymbol{N}]^T[\bar{\boldsymbol{m}}][\boldsymbol{N}]\{\dot{\boldsymbol{d}}^e\}\,\mathrm{d}\boldsymbol{x} \tag{15}$$

where $\boldsymbol{a}_e$ is the length of the element and $\boldsymbol{V}$ is the applied voltage. The various rigidity matrices $[\boldsymbol{D}_b]$, $[\boldsymbol{D}_s]$, and $\{\boldsymbol{D}_{ap}\}$; the mass parameter matrix $\bar{\boldsymbol{m}}$, and the force vector $\{\boldsymbol{f}^s\}$ appearing in Eqs. (14) and (15) are obtained as

$$[\boldsymbol{D}_b] = \sum_{L=1}^{N+2}\int_{h_L}^{h_{L+1}} \boldsymbol{C}_{11}^L[\boldsymbol{Z}]^T[\boldsymbol{Z}]\,\mathrm{d}z, \qquad [\boldsymbol{D}_s] = \sum_{L=1}^{N+2}\int_{h_L}^{h_{L+1}} \boldsymbol{C}_{55}^L\,\mathrm{d}z$$

$$\{\boldsymbol{D}_{ap}\} = \frac{1}{\boldsymbol{h}_p}\int_{h_{N+2}}^{h_{N+3}} [\boldsymbol{Z}]^T[\boldsymbol{e}]\,\mathrm{d}z$$

$$\bar{\boldsymbol{m}} = \sum_{L=1}^{N+2}\int_{h_L}^{h_{L+1}} \rho^L \begin{bmatrix} 1 & 0 & z \\ 0 & 1 & 0 \\ z & 0 & z^2 \end{bmatrix}\mathrm{d}z$$

$$\{\boldsymbol{f}^s\} = [\,0 \quad 1 \quad 0]^T\,\boldsymbol{p}(\boldsymbol{x}, t)$$

Note that because the viscoelastic layer has been modeled by the complex modulus approach, the rigidity matrices $[\boldsymbol{D}_b]$ and $[\boldsymbol{D}_s]$ of an element augmented with the ACLD treatment are complex.

F. Equations of Motion

By application of the principle of virtual work,[26] the following equations of motion for the element are obtained:

$$[\boldsymbol{M}^e]\{\ddot{\boldsymbol{d}}^e\} + [\boldsymbol{K}^e]\{\boldsymbol{d}^e\} = \left\{\boldsymbol{F}_a^e\right\}\boldsymbol{V} + \{\boldsymbol{F}^e\} \tag{16}$$

in which the stiffness matrix $[\boldsymbol{K}^e]$, the mass matrix $[\boldsymbol{M}^e]$, the electroelastic coupling vector $\{\boldsymbol{F}_a^e\}$, and the exciting force vector $\{\boldsymbol{F}^e\}$ of the element are given by

$$[\boldsymbol{K}^e] = \left[\boldsymbol{K}_b^e\right] + \left[\boldsymbol{K}_s^e\right], \qquad \left[\boldsymbol{K}_b^e\right] = \int_0^{a_e} [\boldsymbol{B}_b]^T[\boldsymbol{D}_b][\boldsymbol{B}_b]\,\mathrm{d}\boldsymbol{x}$$

$$\left[\boldsymbol{K}_s^e\right] = \int_0^{a_e} [\boldsymbol{B}_s]^T[\boldsymbol{D}_s][\boldsymbol{B}_s]\,\mathrm{d}\boldsymbol{x}$$

$$[\boldsymbol{M}^e] = \int_0^{a_e} [\boldsymbol{N}]^T[\bar{\boldsymbol{m}}][\boldsymbol{N}]\,\mathrm{d}\boldsymbol{x}, \qquad \left\{\boldsymbol{F}_a^e\right\} = \frac{1}{2}\int_0^{a_e} [\boldsymbol{B}_b]^T\{\boldsymbol{D}_{ap}\}\,\mathrm{d}\boldsymbol{x}$$

$$\{\boldsymbol{F}^e\} = \int_0^{a_e} [\boldsymbol{N}]^T\{\boldsymbol{f}^s\}\,\mathrm{d}\boldsymbol{x}$$

The stiffness matrix of an element augmented with the ACLD treatment is complex because the rigidity matrices involved for the formulation are complex. Note, however, that the equations of motion given by Eq. (16) also represent a typical element without the ACLD

treatment. In that case, the electroelastic coupling vector $\{\boldsymbol{F}_a^e\}$ turns out to be a null vector, and $[\boldsymbol{K}^e]$ becomes real matrix. Also note that to employ the selective integration scheme in a straightforward manner to avoid shear locking, the stiffness matrices $[\boldsymbol{K}_b^e]$ and $[\boldsymbol{K}_s^e]$ associated with the membrane-bending and shear deformations, respectively, are derived separately for an element.

When the continuity conditions given by Eq. (8) are imposed, the degrees of freedom associated with the node of an element in a sublaminate of the delaminated zone lying at the interface between the delaminated zone and an undelaminated zone, can be expressed in terms of those associated with the corresponding node of an element in the sublaminate of the undelaminated zone. This leads to the augmentation of the elemental matrices of that particular element in the delaminated zone before it is assembled. Because there are two sublaminates in the delaminated zone, element matrices of four finite elements in the delaminated zone must to be augmented. For such an element with a leftmost node at the interface, the augmented elemental matrices can be obtained as

$$[\boldsymbol{K}^e]_l = [\boldsymbol{Z}_l]^T[\boldsymbol{K}^e][\boldsymbol{Z}_l], \qquad [\boldsymbol{M}^e]_l = [\boldsymbol{Z}_l]^T[\boldsymbol{M}^e][\boldsymbol{Z}_l]$$
$$\left\{\boldsymbol{F}_a^e\right\}_l = [\boldsymbol{Z}_l]^T\left\{\boldsymbol{F}_a^e\right\}, \qquad \{\boldsymbol{F}^e\}_l = [\boldsymbol{Z}_l]^T\{\boldsymbol{F}^e\} \tag{17}$$

Similarly, for an element with rightmost node at the interface, the augmented elemental matrices can be derived as follows:

$$[\boldsymbol{K}^e]_r = [\boldsymbol{Z}_r]^T[\boldsymbol{K}^e][\boldsymbol{Z}_r], \qquad [\boldsymbol{M}^e]_r = [\boldsymbol{Z}_r]^T[\boldsymbol{M}^e][\boldsymbol{Z}_r]$$
$$\left\{\boldsymbol{F}_a^e\right\}_r = [\boldsymbol{Z}_r]^T\left\{\boldsymbol{F}_a^e\right\}, \qquad \{\boldsymbol{F}^e\}_r = [\boldsymbol{Z}_r]^T\{\boldsymbol{F}^e\} \tag{18}$$

The transformation matrices $[\boldsymbol{Z}_l]$ and $[\boldsymbol{Z}_r]$ in Eqs. (17) and (18) are given by

$$[\boldsymbol{Z}_l] = \begin{bmatrix} 1 & 0 & z_c & 0 & 0 & 0 & 0 & 0 & 0 \\ 0 & 1 & 0 & 0 & 0 & 0 & 0 & 0 & 0 \\ 0 & 0 & 1 & 0 & 0 & 0 & 0 & 0 & 0 \\ 0 & 0 & 0 & 1 & 0 & 0 & 0 & 0 & 0 \\ 0 & 0 & 0 & 0 & 1 & 0 & 0 & 0 & 0 \\ 0 & 0 & 0 & 0 & 0 & 1 & 0 & 0 & 0 \\ 0 & 0 & 0 & 0 & 0 & 0 & 1 & 0 & 0 \\ 0 & 0 & 0 & 0 & 0 & 0 & 0 & 1 & 0 \\ 0 & 0 & 0 & 0 & 0 & 0 & 0 & 0 & 1 \end{bmatrix}$$

$$[\boldsymbol{Z}_r] = \begin{bmatrix} 1 & 0 & 0 & 0 & 0 & 0 & 0 & 0 & 0 \\ 0 & 1 & 0 & 0 & 0 & 0 & 0 & 0 & 0 \\ 0 & 0 & 1 & 0 & 0 & 0 & 0 & 0 & 0 \\ 0 & 0 & 0 & 1 & 0 & 0 & 0 & 0 & 0 \\ 0 & 0 & 0 & 0 & 1 & 0 & 0 & 0 & 0 \\ 0 & 0 & 0 & 0 & 0 & 1 & 0 & 0 & 0 \\ 0 & 0 & 0 & 0 & 0 & 0 & 1 & 0 & z_c \\ 0 & 0 & 0 & 0 & 0 & 0 & 0 & 1 & 0 \\ 0 & 0 & 0 & 0 & 0 & 0 & 0 & 0 & 1 \end{bmatrix}$$

The elemental equations are assembled to obtain the global equations of motion governing the open-loop behavior of the beam as follows:

$$[\boldsymbol{M}]\{\ddot{\boldsymbol{X}}\} + [\boldsymbol{K}]\{\boldsymbol{X}\} = \{\boldsymbol{F}_a\}\boldsymbol{V} + \{\boldsymbol{F}\} \tag{19}$$

where $[\boldsymbol{M}]$ is the global mass matrix, $[\boldsymbol{K}]$ is the global stiffness matrix, $\{\boldsymbol{X}\}$ are the global nodal degrees of freedom, $\{\boldsymbol{F}\}$ is the global nodal force vector, and $\{\boldsymbol{F}_a\}$ is the global electroelastic coupling vector. Recall that $[\boldsymbol{K}^e]$ is complex for the element augmented with ACLD treatment. Then one can realize that the global stiffness matrix $[\boldsymbol{K}]$ turns out to be a complex stiffness matrix, and its imaginary part contributes to the dissipation of energy. Hence, if the piezoelectric constraining layer is passive, that is, $\boldsymbol{V} = 0$, the equation of motion given by Eq. (19) governing the open-loop behavior represents the modeling of the passive constrained layer damping of the overall system.[27,28]

III. Closed-Loop Model

To activate the piezoelectric constraining layer of the patch, a simple velocity feedback strategy has been simulated. The control law considers that the piezoelectric constraining layer is subjected to a control voltage proportional to the transverse velocity at the free end of the patch. Thus, the control voltage for the actuator can be expressed in terms of the derivatives of the nodal global degrees of freedom, as follows:

$$\boldsymbol{V} = -\boldsymbol{K}_d[\boldsymbol{r}]\{\dot{\boldsymbol{X}}\} \tag{20}$$

where $\boldsymbol{K}_d$ is the control gain for the actuator and $[\boldsymbol{r}]$ is a position vector defining the location of the point of sensing the velocity.

Finally, substitution of Eq. (20) into (19) yields the equations of motion governing the closed-loop dynamics of the beams with or without delaminations and augmented with the activated patch of ACLD treatment, as follows:

$$[\boldsymbol{M}]\{\ddot{\boldsymbol{X}}\} + [\boldsymbol{C}_d]\{\dot{\boldsymbol{X}}\} + [\boldsymbol{K}]\{\boldsymbol{X}\} = \{\boldsymbol{F}\} \tag{21}$$

where $[\boldsymbol{C}_d] = \{\boldsymbol{F}_a\}[\boldsymbol{r}]$ is the active damping matrix. Note that if $\boldsymbol{K}_d = 0$, Eq. (21) reduces to Eq. (19), representing the passive constrained layer damping of the overall system. Hence, for $\boldsymbol{K}_d \neq 0$, Eq. (21) represents the modeling of the composite beams integrated with the patch of ACLD treatment undergoing both active and passive damping simultaneously, which is the essence of ACLD.

IV. Modeling of Sensor

The piezoelectric layer attached at the bottom surface of the beam deforms as a result of the deformations of the beam due to external excitation. This deformation results in the generation of induced charge in the piezoelectric layer by virtue of direct piezoelectric effect. Because the piezoelectric layer is coated with surface electrodes, the induced charges at the bottom surface of the sensor layer can be accumulated at the bottom surface electrode of the layer. With proper arrangement of hardware, this accumulated charge can provide the measure of deformation of the beam.

The constitutive equation governing the direct piezoelectric effect in the sensor layer is given by

$$\boldsymbol{D}_z = \boldsymbol{e}_{31}\varepsilon_x + \in_{33}\boldsymbol{E}_z \tag{22}$$

where $\boldsymbol{D}_z$ is the electric displacement in the z direction and $\in_{33}$ is the dielectric constant of the piezoelectric material. The sensor layer is not subjected to any externally applied electric field, and the converse effect of the weak electric field due to the induced charges developed in the sensor layer can be neglected. Thus, the total charge $\boldsymbol{q}$ per unit width of the sensor layer induced at its bottom surface can be expressed as

$$\boldsymbol{q} = \int_0^{a_p} \boldsymbol{D}_z|_{z=-(h_p+h/2)}\,\mathrm{d}\boldsymbol{x} \tag{23}$$

in which $\boldsymbol{a}_p$ is the length of the piezoelectric sensor layer. By the use of Eqs. (2), (12), (13), and (22) in Eq. (23), the induced charge per unit width of $\boldsymbol{e}$th typical element can be expressed as

$$\boldsymbol{q}^e = \boldsymbol{e}_{31}\left[\boldsymbol{K}_{\text{sen}}^e\right]\{\boldsymbol{d}^e\} \tag{24}$$

where

$$\left[\boldsymbol{K}_{\text{sen}}^e\right] = \int_0^{a_e} [\boldsymbol{Z}_s][\boldsymbol{B}_b]\,\mathrm{d}\boldsymbol{x}, \qquad [\boldsymbol{Z}_s] = \left[1 \quad -\left(\frac{\boldsymbol{h}}{2} + \boldsymbol{h}_p + z_c\right)\right]$$

Integration of the elemental induced charge given by Eq. (24) over the length of the sensor layer yields the total induced charge collected at the bottom surface electrode of the sensor layer. It can be

expressed as

$$q = \sum_{e=1}^{m} q^e \tag{25}$$

where m is the number of elements being integrated with the sensor layer.

V. Numerical Results and Discussion

In this section, the numerical results for the effect of delamination on the performance of ACLD treatment has been demonstrated with the finite element model derived in the previous section. For the purpose of verifying the finite element model, the beams already studied by earlier researchers[39] have been considered as the load bearing part of the smart beams. Single and centrally located delamination is considered for verification of the model. The material properties of the orthotropic layers of the beams are[39] $E_1 = 172.5$ GPa, $E_3 = 11.7$ GPa, $G_{13} = 4.8$ GPa, $\upsilon_{13} = 0.24$, and $\rho = 1578$ kg/m^3, where the symbols have the usual meaning. The commercially available viscoelastic sheet (DYAD 606) is considered for the numerical results. The shear modulus, Poisson's ratio, and the density of this viscoelastic material are $20(1+i)$ MN/m^2, 0.25, and 1140 kg/m^3, respectively.[25] Also, the loss factor ($\eta = 1.0$) of this viscoelastic material remains approximately constant over the frequency range of interest from 0 to 800 Hz. The piezoelectric material is a uniaxially polarized polymeric film (PVDF) and is elastically isotropic. Its Young's modulus, Poisson's ratio, and density are 2.25 GN/m^2, 0.28, and 1800 kg/m^3, respectively.[25] For PVDF, the value of the piezoelectric constant (e_{31}) is 0.046 C/m^2. The length and thickness of the beams are 0.2794 m and 1.016 mm, respectively. The thickness of the viscoelastic layer is 1.0 mm and that of the piezoelectric layers is 28 μm. When the finite element model derived here is used, the natural frequencies are first computed for untreated beams without and with the presence of delamination and are compared with the existing results, as presented in Tables 1 and 2. A very good agreement can be observed from Tables 1 and 2. As expected, the delamination causes a decrease in the natural frequencies corresponding to higher modes.

To investigate the effect of delaminations on the performance of ACLD treatment, numerically evaluated FRFs of the smart beams are examined when the beams are excited with a time harmonic force at their free ends. By employment of the mechanical impedance approach, Eq. (21) can be formulated to compute the numerical data for the FRFs of the beams. For all of the numerical responses, the length of the ACLD treatment, as well as that of the sensor layer, is considered as 40% of the length of the beams. The response will be treated as active or passive according to whether the piezoelectric constraining layer of the ACLD treatment is subjected to control voltage or not. For evaluation of the active response, the magnitude of the control gain used is 20,000. When the numerical values of the generalized nodal degrees of freedom in Eq. (25) are substituted, the total charge induced at the bottom surface of the sensor layer can be computed for a frequency of excitation. The plot for the variation of this induced charge with the excitation frequency illustrates the frequency response of the sensor layer.

Table 1 Comparison of natural frequencies (hertz) of [0/90/45/−45]s cantilever beam

Source	%Delamination	Mode 1	Mode 2	Mode 3	Mode 4
Present	0	17.79	111.2	311.9	611.4
Ref. 34		17.75	110.3	318.7	611.7
Present	20	17.2	110.2	277.1	585.3
Ref. 34		17.70	108.2	278.0	582.1
Present	40	17.0	93.1	197.6	398.2
Ref. 34		17.5	92.1	200.0	400.0

Table 2 Comparison of natural frequencies (hertz) of [45/−45/90/0]s cantilever beam

Source	%Delamination	Mode 1	Mode 2	Mode 3	Mode 4
Present	0	10.5	65.8	184.2	365.2
Ref. 34		10.3	65.4	188.3	367.2
Present	20	10.3	65.7	175.5	322.8
Ref. 34		10.3	65.4	176.2	324.2
Present	40	10.2	62.0	148.2	272.0
Ref. 34		10.3	63.1	150.0	274.0

Given centrally located 20% delamination at the middle plane of the [0/90/45/−45]s cantilever beam, the transverse displacement at its free end is computed as a function of frequency, shown in Fig. 2. Figure 2 also contains the response of the beam without delamination. The corresponding induced charge at the bottom surface of the sensor layer is plotted in Fig. 3. The control input also needs to be monitored to assess the health of a smart structure. Hence, the control voltage required to obtain the active response of this beam has been computed and is shown in Fig. 4. The FRF data for the transverse displacement at the free end of the [45/−45/90/0]s cantilever beam with and without the presence of delamination is shown in Fig. 5. In this case as well, 20% delamination at the middle plane of the beam is considered. The response of the sensor layer of this beam and the required control voltage are shown in Figs. 6 and 7, respectively.

Note from the plots of transverse displacement presented in Figs. 2 and 5 that when the ACLD treatment is in operation, the response of the delaminated beam deviates from that of the beam without delamination, particularly for higher modes. When compared with the active response of undelaminated beam, the active response of delaminated beam shows a decrease in the natural frequencies for

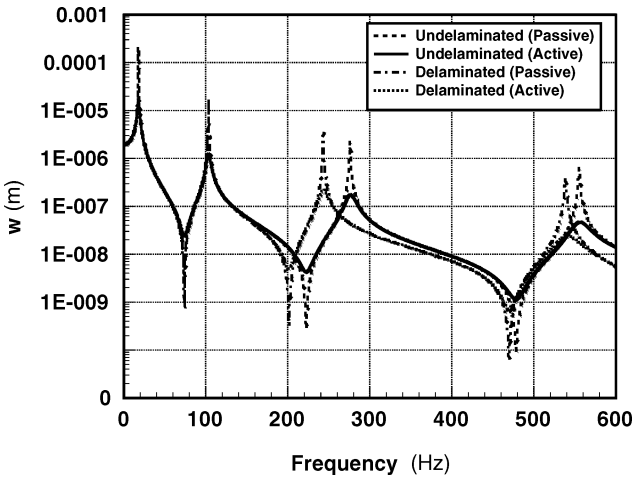

Fig. 2 Frequency response of a [0/90/45/−45]s cantilever beam with 20% delamination at the middle of the beam.

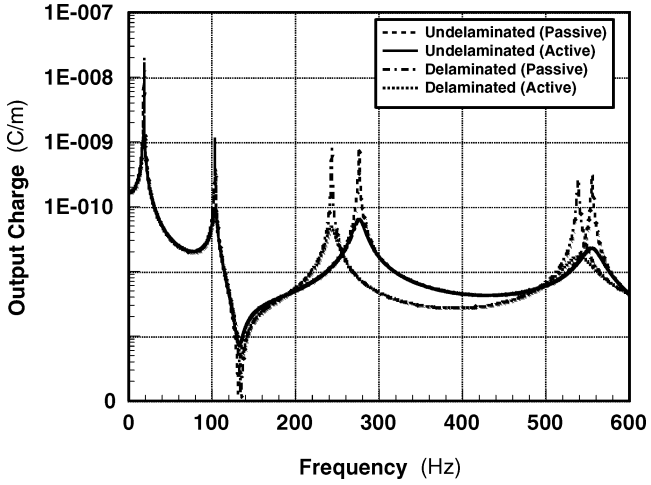

Fig. 3 Frequency response of the sensor layer of a [0/90/45/−45]s cantilever beam with 20% delamination at the middle of the beam.

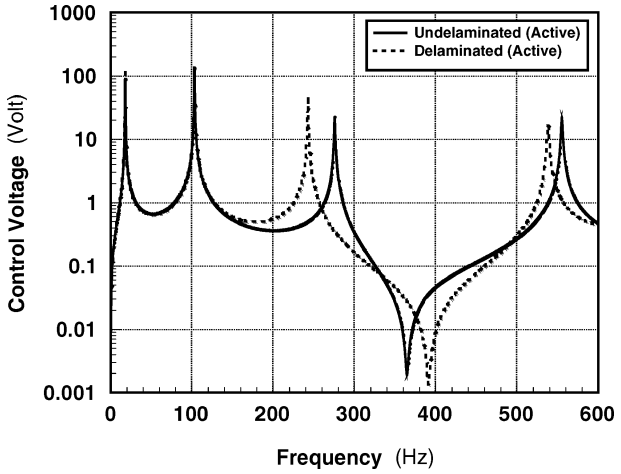

Fig. 4 Control voltage for a [0/90/45/−45]$_s$ cantilever beam with and without 20% delamination at the middle of the beam.

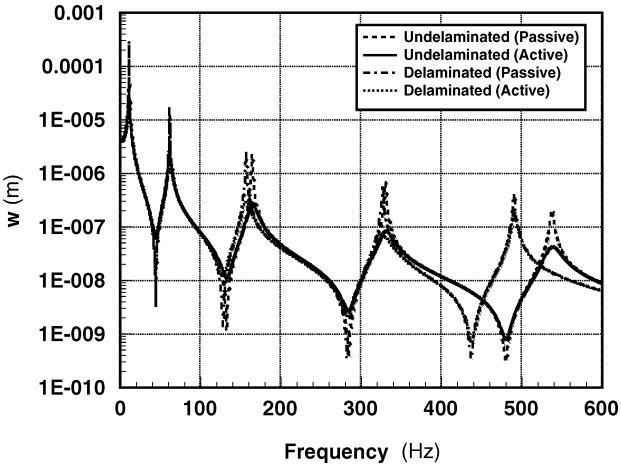

Fig. 5 Frequency response of a [45/−45/90/0]$_s$ cantilever beam with 20% delamination at the middle of the beam.

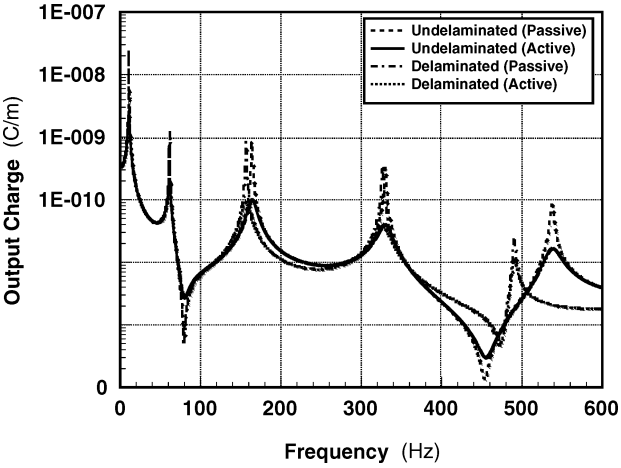

Fig. 6 Frequency response of the sensor layer of a [45/−45/90/0]$_s$ cantilever beam with 20% delamination at the middle of the beam.

the higher modes. Hence, to understand the cause of decrease in natural frequencies observed in the active response of the delaminated beams, the passive response has also been presented in Figs. 2 and 5. Note that both active and passive responses indicate the lowering of higher natural frequencies by the same amount due to the presence of delamination. In the present investigation, the derivative controller has been used to activate the ACLD treatment, and it does not result in frequency shifting. Thus, as long as the active

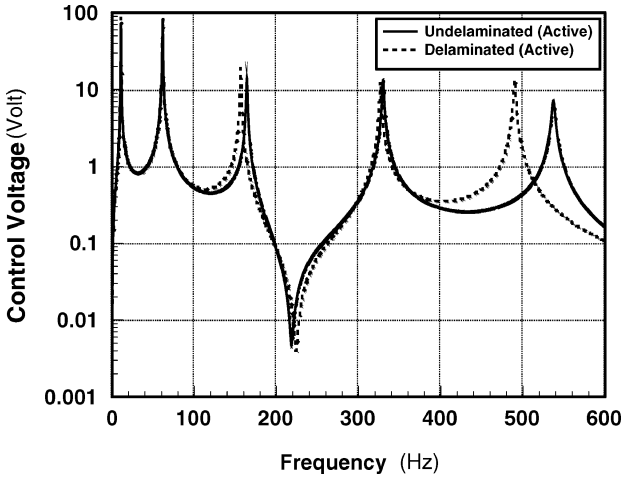

Fig. 7 Control voltage for a [45/−45/90/0]$_s$ cantilever beam with 20% delamination at the middle of the beam.

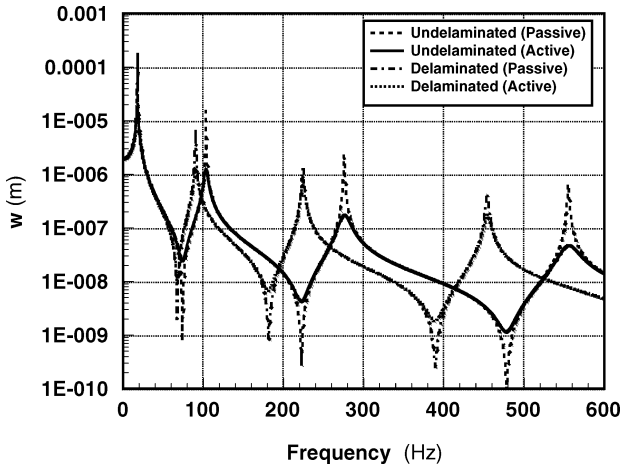

Fig. 8 Frequency response of a [0/90/45/−45]$_s$ cantilever beam with 20% delamination at the fixed end ($x = 0$) of the beam.

response of a smart laminated beam is monitored, the cause of decrease in the natural frequencies for higher modes can be attributed to one of the imperfections such as the occurrence of delamination in the beam. Comparison of Figs. 2–4 with Figs. 5–7 reveals that the responses are more sensitive to the presence of delamination in the case of a [0/90/45/−45]$_s$ beam than a [45/−45/90/0]$_s$ beam for small delamination (say 20%). It has been reported[39] that the effect of delamination on the modal characteristics of a [45/−45/90/0]$_s$ cantilever beam not integrated with ACLD treatment is quite modest and is not even perceptible for small delamination such as 20%. However, the present investigation indicates that the performance of ACLD treatment may be exploited to identify the presence of small delamination even in this beam as shown in Figs. 5–7. By the use of Eq. (25), the computation of induced charge does not explicitly depend on the transverse displacement of the beam. Notice from Figs. 3 and 6, however, that in conformity with the active frequency response for transverse displacement, the output of the sensor layer is also affected due to the presence of delamination. For a particular control gain, when the active responses for the transverse displacement at the free end of the beams are compared, note that almost the same attenuation of vibrations has been achieved for both delaminated and undelaminated beams. Hence, the performance of the ACLD treatment is not degraded due to the presence of the delamination at the center of the beams within the frequency range (0–600 Hz) considered in this study.

The frequency responses of the beams with delaminations at different locations other than the center are shown in Figs. 8–11. Figures 8 and 9 demonstrate the transverse displacement at the free

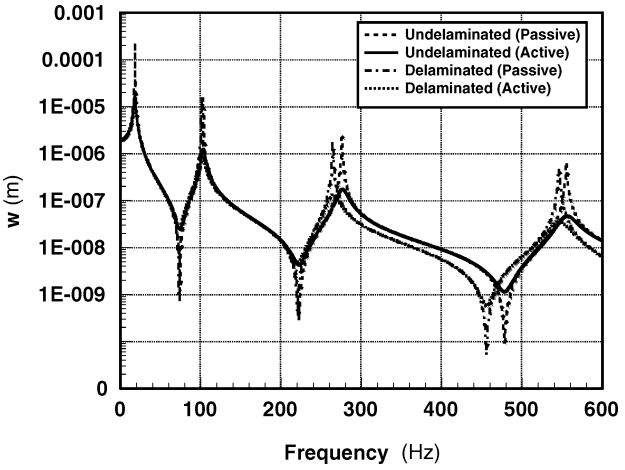

Fig. 9 Frequency response of the [0/90/45/−45]*s* cantilever beam with 20% delamination near the free end ($x = 0.7a$) of the beam.

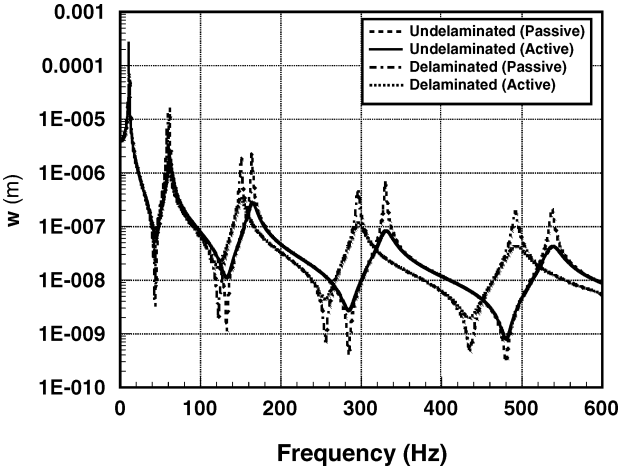

Fig. 10 Frequency response of a [45/−45/90/0]*s* cantilever beam with 20% delamination at the fixed end ($x = 0$) of the beam.

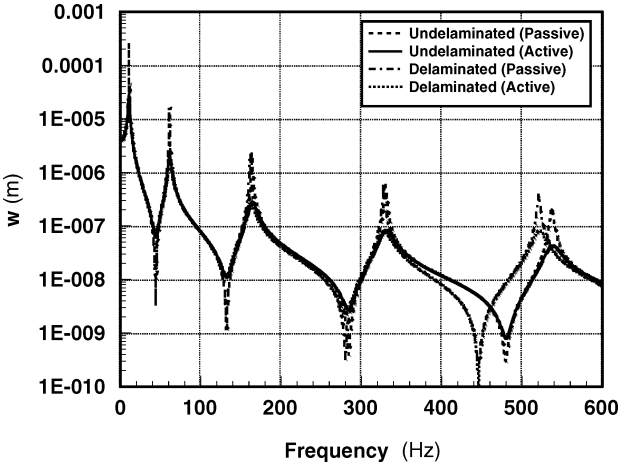

Fig. 11 Frequency response of a [45/−45/90/0]*s* cantilever beam with 20% delamination near the free end ($x = 0.7a$) of the beam.

end of a [0/90/45/−45]*s* beam when the start of delamination is located at the fixed end ($x = 0$) and near the free end ($x = 0.7a$) of the beam, respectively. Again, 20% delamination has been considered to compute the responses. Note that when the responses presented in Figs. 2, 8, and 9 are compared, the number of modes being affected by the presence of delamination is at a maximum when the delamination is located at the fixed end of the beam. When compared with the pristine beam, the performance of the ACLD treatment has not been affected much by the presence of delamination located near the free end of the beam, as manifested by the response presented in Fig. 9. A similar trend of results is also obtained for a [45/−45/90/0]*s* beam, shown in Figs. 5, 10, and 11.

VI. Conclusions

In this paper, the performance of the ACLD treatment in smart laminated composite beams containing small delamination at various locations has been theoretically investigated. Two eight-layered cantilevered composite beams with lamination schemes [0/90/45/−45]*s* and [45/−45/90/0]*s* have been considered as the base structures of the smart beams. The beams are integrated with a patch of ACLD treatment on their top surfaces and a patch of piezoelectric film acting as a distributed sensor layer at their bottom surfaces. Both the patch of the treatment and the sensor layer are placed at the fixed end of the beams. A finite element model has been developed to describe the open- and closed-loop dynamics of the beams with and without the presence of delamination. When compared with the pristine beams, the active and passive responses of the delaminated beams exhibit significant deviations, particularly at higher modes. The lower modes are also highly effected when the delamination is located near the fixed end of the beams. The effect of small delamination (20%) on the damped dynamic characteristics is not at all perceptible for the beam with lamination scheme [45/−45/90/0]*s* as studied by the earlier researchers.[39] However, the present study reveals that the performance of ACLD treatment is also able to exhibit the presence of small delamination in this beam. The effect of delamination is also manifested in the frequency responses of the sensor layer and control voltage in conformity with the transverse displacement. The active frequency responses indicate that, although delamination causes reduction in stiffness of the beams, the ACLD treatment is capable of improving the damping characteristics of the delaminated beams. Hence, the results of the present study provide an important conclusion: When ACLD treatment is under operation, the achievement of improved damping in a smart laminated composite structure does not necessarily mean that the structure is perfect. Also, the frequency responses obtained in this investigation may provide useful a priori knowledge to detect the presence of delamination in smart composite beams by the use of the existing numerical techniques.

Acknowledgments

The research reported herein was carried out under the U.S. Army Research Office Grant DAAD19-01-1-0483. The support and encouragement by Gary Anderson is gratefully acknowledged.

References

[1]Bailey, T., and Hubbard, J. E., "Distributed Piezoelectric Polymer Active Vibration Control of a Cantilever Beam," *Journal of Guidance, Control, and Dynamics*, Vol. 8, No. 2, 1985, pp. 605–611.

[2]Crawley, E. F., and Luis, J. D., "Use of Piezoeletric Actuators as Elements of Intelligent Structures," *AIAA Journal*, Vol. 25, 1987, pp. 1373–1385.

[3]Baz, A., and Poh, S., "Performance of an Active Control System with Piezoelectric Actuators," *Journal of Sound and Vibration*, Vol. 126, 1988, pp. 327–343.

[4]Tzou, H. S., and Tseng, C. I., Distributed Piezoelectric Sensor/Actuator Design for Dynamic Measurement/Control of Distributed Parameter Systems: A Piezoelectric Finite Element Approach," *Journal of Sound and Vibration*, Vol. 138, 1990, pp. 17–34.

[5]Lee, C. K., Chiang, W. W., and Sulivan, O., "Piezoelectric Modal Sensor/Actuator Pairs for Critical Active Damping Vibration Control," *Journal of Accoustical Society of America*, Vol. 90, 1991, pp. 374–384.

[6]Hanagud, S., Obal, M. W., and Calise, A. J., "Optimal Vibration Control by the Use of Piezoceramic Sensors and Actuators," *Journal of Guidance, Control, and Dynamics*, Vol. 15, 1992, pp. 1199–1206.

[7]Chandrashekara, K., and Agarwal, A. N., "Active Vibration Control of Laminated Composite Plates Using Piezoelectric Devices: A Finite Element Approach," *Journal of Intelligent Materials, Systems and Structures*, Vol. 4, 1993, pp. 496–508.

[8]Ray, M. C., Bhattacharyya, R., and Samanta, B., "Exact Solutions for Static Analysis of Intelligent Structures," *AIAA Journal*, Vol. 31, 1993, pp. 1684–1691.

[9]Gu, Y., Clark, R. L., and Fuller, C. R., "Experiments on Active Control of Plate Vibration Using Piezoelectric Actuators and Polyvinylidyne Fluoride (PVDF) Modal Sensors," *Journal of Vibration and Acoustics*, Vol. 116, 1994, pp. 303–308.

[10]Zhou, R. C., Lai, Z., Xue, D. Y., Huang, J. K., and Mei, C., "Suppression of Nonlinear Panel Flutter with Piezoelectric Actuators Using Finite Element Method," *AIAA Journal*, Vol. 6, 1995, pp. 1098–1105.

[11]Ray, M. C., Samanta, B., and Bhattacharyya, R., "Finite Element Model for Active Control of Intelligent Structures," *AIAA Journal*, Vol. 34, 1996, pp. 1885–1893.

[12]Baz, A., and Poh, S., "Optimal Vibration Control with Modal Positive Position Feedback," *Optimal Control Applications and Methods*, Vol. 17, 1996, pp. 141–149.

[13]Varadan, V. V., Kim, J., and Varadan, V. K., "Optimal Placement of Piezoelectric Actuators for Active Noise Control," *AIAA Journal*, Vol. 35, 1997, pp. 526–533.

[14]Seifert, A., Eliahu, S., Greenblatt, D., and Wygnanski, I., "Use of Piezoelectric Actuators for Airfoil Separation Control," *AIAA Journal*, Vol. 36, 1998, pp. 1535–1537.

[15]Ray, M. C., "Optimal Control of Laminated Plates with Piezoelectric Sensor and Actuator Layers," *AIAA Journal*, Vol. 12, 1998, pp. 2204–2208.

[16]Agarwal, B. N., and Treanor, K. E., "Shape Control of a Beam Using Piezoelectric Actuators," *Smart Materials and Strutctures*, Vol. 8, 1999, pp. 729–740.

[17]Barboni, R., Mannini, A., Fantini, E., and Gaudenzi, P., "Optimal Placement of PZT Actuators for the Control of Beam Dynamics," *Smart Materials and Strutctures*, Vol. 9, 2000, pp. 110–120.

[18]Dong, S., and Tong, L., "Vibration Control of Plates Using Discretely Distributed Piezoelectric Quasi-Modal Actuators/Sensors," *AIAA Journal*, Vol. 39, 2001, pp. 1766–1772.

[19]Ray, M. C., "Optimal Control of Laminated Shells Using Piezoelectric Sensor and Actuator Layers," *AIAA Journal*, Vol. 41, No. 6, 2003, pp. 1151–1157.

[20]Mukherjee, A., and Joshi, S., "Piezoelectric Sensor and Actuator Design for Shape Control of Piezolaminated Plates," *AIAA Journal*, Vol. 40, 2002, pp. 1204–1210.

[21]Baz, A., and Ro, J., "Optimum Design and Control of Active Constrained Layer Dmping," *Journal of Vibration and Acoustics*, Vol. 117B, 1995, pp. 135–144.

[22]Azvine, B., Tomlinson, G. R., and Wynne, R. J., "Use of Active Constrained Layer Damping for Controlling Resonant," *Smart Materials and Structures*, Vol. 4, 1995, pp. 1–6.

[23]Ray, M. C., and Baz, A., "Optimization of Energy Dissipation of Active Constrained Layer Damping Treatments of Plates," *Journal of Sound and Vibration*, Vol. 208, 1997, pp. 391–406.

[24]Ray, M. C., and Baz, A., "Control of Nonlinear Vibration of Beams Using Active Constrained Layer Damping Treatment," *Journal of Vibration and Control*, Vol. 7, 2001, pp. 539–549.

[25]Ray, M. C., Oh, J., and Baz, A., "Active Constrained Layer Damping of Thin Cylindrical Shells," *Journal of Sound and Vibration*, Vol. 240, No. 5, 2001, pp. 921–935.

[26]Jeung, Y. S., and Shen, I. Y., "Development of Isoparametric, Degenerate Constrained Layer Element for Plate and Shell Structures," *AIAA Journal*, Vol. 39, No. 10, 2001, pp. 1997–2005.

[27]Chantalakhana, C., and Stanway, R., "Active Constrained Layer Damping of Clamped–Clamped Plate Vibrations," *Journal of Sound and Vibration*, Vol. 241, No. 5, 2001, pp. 755–777.

[28]Ro, J., and Baz, A., "Optimum Placement and Control of Active Constrained Layer Damping Using Modal Strain Energy Approach," *Journal of Vibration and Control*, Vol. 8, 2002, pp. 861–876.

[29]Liu, Y., and Wang, K-W., "Enhanced Active Constrained Layer Damping Treatment for Broadband Vibration Suppression," *Journal of Vibration and Control*, Vol. 8, 2002, pp. 777–803.

[30]Gandhi, F., and Munskey, B. E., "Comparison of Damping Augmentation Mechanisms with Position and Velocity Feedback in Active Constrained Layer Treatments," *Journal of Intelligent Materials, Systems and Structures*, Vol. 13, No. 5, 2002, pp. 326–335.

[31]Ratcliffe, C. P., and Bagaria, W. J., "Vibration Technique for Locating Delamination in a Composite Beam," *AIAA Journal*, Vol. 36, No. 6, 1998, pp. 1074–1077.

[32]Kawiecki, G., "Modal Damping Measurement for Damage Detection," *Smart Materials and Structures*, Vol. 10, 2001, pp. 466–471.

[33]Kawiecki, G., and Jesse, S., "Rosette Piezotransducers for Damage Detection," *Smart Materials and Structures*, Vol. 11, 2002, pp. 196–201.

[34]Kessler, S. S., Spearing, S. M., Atalla, M. J., Cesnik, C., and Soutis, C., "Damage Detection in Composite Materials Using Frequency Response Methods," *Composites Part B: Engineering*, Vol. 33, 2002, pp. 87–95.

[35]Thyagarajan, S. K., Schulz, M. J., and Pai, P. F., "Detecting Structural Damage Using Frequency Response Functions," *Journal of Sound and Vibration*, Vol. 210, 1998, pp. 162–170.

[36]Wang, Z., Lin, R. M., and Lim, M. K., "Structural Damage Detection Using Measured FRF Data," *Computational Methods in Applied Mechanics and Engineering*, Vol. 147, 1997, pp. 187–197.

[37]Chattopadhyay, A., Daescu, D. D., and Gu, H., "Dynamics of Delaminated Smart Composite Cross-Ply Beams," *Smart Materials and Structures*, Vol. 8, 1999, pp. 92–99.

[38]Nashif, A., Jones, D. I., and Henderson, J. P., *Vibration Damping*, Wiley, New York, 1985.

[39]Saravanos, D. A., and Hopkins, D. A., "Effects of Delaminations on the Damped Dynamic Characteristics of Composite Laminates: Analysis and Experiments," *Journal of Sound and Vibration*, Vol. 192, 1996, pp. 977–993.

A. Chattopadhyay
Associate Editor